J. Am. Soc. Mass Spectrom. (2016) 27:1846–1854
DOI: 10.1007/s13361-016-1468-z

RESEARCH ARTICLE

Collision-Induced Dissociation of Electrosprayed NaCl Clusters: Using Molecular Dynamics Simulations to Visualize Reaction Cascades in the Gas Phase

Tilo D. Schachel, Haidy Metwally, Vlad Popa, Lars Konermann

Department of Chemistry, The University of Western Ontario, London, ON N6A 5B7, Canada

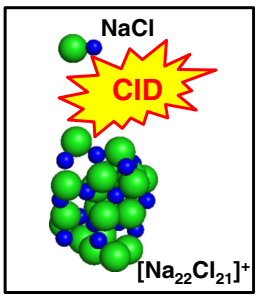

Abstract. Infusion of NaCl solutions into an electrospray ionization (ESI) source produces $[Na_{(n+1)}Cl_n]^+$ and other gaseous clusters. The $n = 4$, 13, 22 magic number species have cuboid ground state structures and exhibit elevated abundance in ESI mass spectra. Relatively few details are known regarding the mechanisms whereby these clusters undergo collision-induced dissociation (CID). The current study examines to what extent molecular dynamics (MD) simulations can be used to garner insights into the sequence of events taking place during CID. Experiments on singly charged clusters reveal that the loss of small neutrals is the dominant fragmentation pathway. MD simulations indicate that the clusters undergo extensive structural fluctuations prior to decomposition. Consistent with the experimentally observed behavior, most of the simulated dissociation events culminate in ejection of small neutrals ($[NaCl]_i$, with $i = 1$, 2, 3). The MD data reveal that the prevalence of these dissociation channels is linked to the presence of short-lived intermediates where a relatively compact core structure carries a small $[NaCl]_i$ protrusion. The latter can separate from the parent cluster via cleavage of a single Na-Cl contact. Fragmentation events of this type are kinetically favored over other dissociation channels that would require the quasi-simultaneous rupture of multiple electrostatic contacts. The CID behavior of NaCl cluster ions bears interesting analogies to that of collisionally activated protein complexes. Overall, it appears that MD simulations represent a valuable tool for deciphering the dissociation of noncovalently bound systems in the gas phase.

Keywords: Reaction mechanism, Salt cluster, Transition state, Charged residue model, Magic number

Received: 24 May 2016/Revised: 28 July 2016/Accepted: 29 July 2016/Published Online: 8 September 2016

Introduction

Electrospray ionization (ESI) of solutions containing nonvolatile salts produces gaseous cluster ions [1–7]. These clusters are widely used as mass spectrometry (MS) calibrants [8]. Salts such as NaCl are strong electrolytes (i.e., in bulk aqueous solution they exist as hydrated Na^+ and Cl^- entities that are completely separated from one another [9]). The observation of $[Na_xCl_y]^{(x-y)+}$ clusters in ESI mass spectra obtained from such solutions thus represents a remarkable phenomenon. ESI-mediated clustering also takes place for amino acids and other low molecular weight solutes [10–13].

Salt clusters continue to play a central role for mechanistic investigations of the ESI process [5, 14, 15]. It has been suggested that these clusters self-assemble in the super-saturated environment of rapidly shrinking ESI droplets [3, 16]. Depending on their physicochemical properties, some clusters may be released from the droplet via the ion evaporation mechanism (IEM) [5, 17], in a manner that is analogous to the ESI process of monoatomic ions [18–21]. However, it is believed that most salt clusters (including $[Na_xCl_y]^{(x-y)+}$) are produced by solvent evaporation to dryness [22–24], as envisioned by the charged residue model (CRM) [25, 26]. Similar CRM clustering phenomena appear to be responsible for the nonspecific salt adduction to proteins and other macromolecular analytes, generating heterogeneous species such as $[M + zH + n(Na - H) + m(Cl + H)]^{z+}$ [27–29]. Some of these mixed salt/protein species have been shown to exhibit remarkable structural stability, thereby renewing general interest in ESI-mediated clustering events [30–33].

One particularly intriguing aspect is the prevalence of salt clusters with specific "magic number" compositions [11–13, 34–36].

Electronic supplementary material The online version of this article (doi:10.1007/s13361-016-1468-z) contains supplementary material, which is available to authorized users.

Correspondence to: Lars Konermann; *e-mail:* konerman@uwo.ca

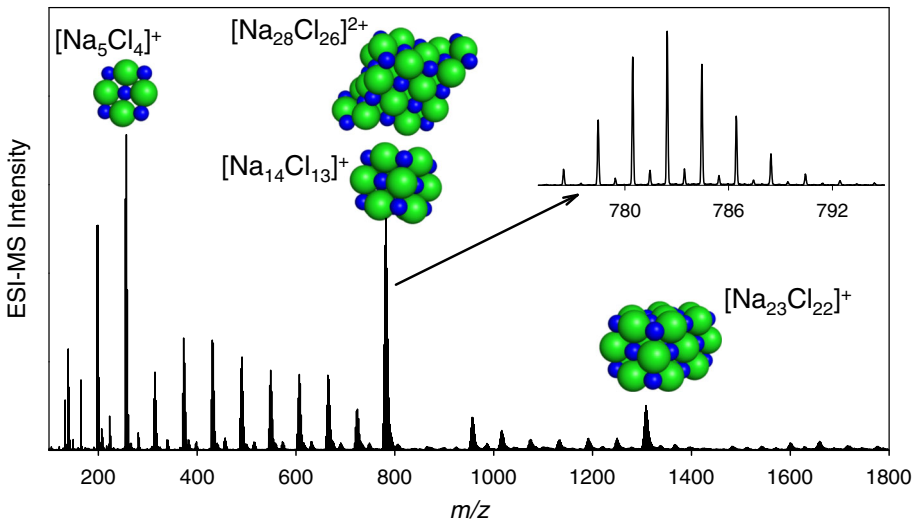

Figure 1. Positive ion ESI mass spectrum obtained by electrospraying aqueous NaCl solution at a cone voltage of 75 V. The inset shows the region around *m/z* 785 at a cone voltage of 15 V, where both singly charged (major signals) and doubly charged (minor peaks) clusters are observable. Also shown are the ground state structures of the corresponding cluster ions, obtained after energy minimization and annealing of the magic number combinations $[Na_{(n+1)}Cl_n]^+$ for $n = 4$, 13, and 22, as well as $[Na_{28}Cl_{26}]^{2+}$

For example, ESI of NaCl solutions in positive ion mode produces particularly strong $[Na_{(n+1)}Cl_n]^+$ signals for $n = 4$, 13, and 22, which may be envisioned as cuboids consisting of $(3 \times 3 \times 1)$, $(3 \times 3 \times 3)$, and $(3 \times 3 \times 5)$ ions, respectively [1, 22, 37, 38]. The missing magic number species in this series [$(3 \times 3 \times 2)$ and $(3 \times 3 \times 4)$] are neutral and therefore unobservable by MS. Multiply charged clusters have ground state geometries that are more complicated than the cuboids seen for small singly charged species [39].

While the mechanism of salt cluster formation during ESI has received major attention, much less is known about the dissociation of these species following activation in the gas phase. Collision-induced dissociation (CID) remains the most widely used MS/MS fragmentation method. CID relies on collisions with neutral background gas to increase the internal energy of the analyte, until the system is able to overcome activation barriers for decomposition [40–42]. Feketeova and O'Hair [43] examined the CID behavior of various $[Na_{(n+1)}Cl_n]^+$ clusters. Fragmentation was found to proceed via loss of neutral $[NaCl]_i$ moieties, but it was not clear whether these ejected species corresponded to individual NaCl molecules ($i = 1$) or clusters with $i > 1$. Evidence for the occurrence of neutral losses with $i = 1$ comes from dissociation experiments on various other types of salt clusters conducted on differential mobility analysis instruments [7, 44]. Zhang and Cooks [34] conducted CID measurements on doubly charged $[Na_{(n+2)}Cl_n]^{2+}$ magic number clusters. Larger clusters dissociated via neutral losses, whereas smaller clusters were found to dissociate into singly charged magic number species. It was suggested that these magic number products arise from parent species consisting of preformed magic number $[Na_{(n+1)}Cl_n]^+$ crystalloids, which separate from each other along simple fracture planes. For example, the authors proposed that $[Na_{28}Cl_{26}]^{2+}$ is composed of a $(3 \times 3 \times 1)^+$ and a $(5 \times 3 \times 3)^+$ unit [34]. This interpretation implies that fragments retain structural features of the precursor ground state geometries.

The view of structural retention during CID of NaCl clusters seems at odds with ion mobility spectrometry (IMS) results of Hudgins et al. [45], which revealed extensive changes in cluster shape prior to the onset of dissociation. The pliability of salt clusters seen by IMS is in line with theoretical investigations, which reveal that NaCl nanocrytals can easily deform, a feature that is very different from the brittle properties of bulk NaCl [37]. Also, Coulombic modeling suggests that cuboid ground state structures are only marginally more stable than some distorted isomers [38]. This brief discussion highlights the fact that much remains to be learned about the CID mechanism of NaCl clusters.

In addition to experimental studies, molecular dynamics (MD) simulations are increasingly being used to probe mechanistic aspects of the ESI process [19, 24, 46–48], as well as the fate of desolvated analytes in the gas phase [49–56]. Standard MD force fields do not allow for the rupture of covalent bonds, whereas modeling the disruption of electrostatic interactions and other noncovalent linkages is straightforward [48, 51, 54]. Hence, MD methods should be well suited for studying the dissociation of gaseous salt clusters, thereby generating "molecular movies" of the CID process. MD simulations have been used extensively for probing physicochemical aspects of NaCl in solution [57–59], as well as the CRM formation of NaCl clusters within ESI droplets [24]. Surprisingly, it appears that there have been no attempts to use MD techniques for probing the fate of salt clusters in the gas phase under CID conditions.

In the current work, we conduct experiments to interrogate the CID behavior of various NaCl clusters over a wide range of collision energies, both in positive and in negative ion mode. Fragmentation proceeds

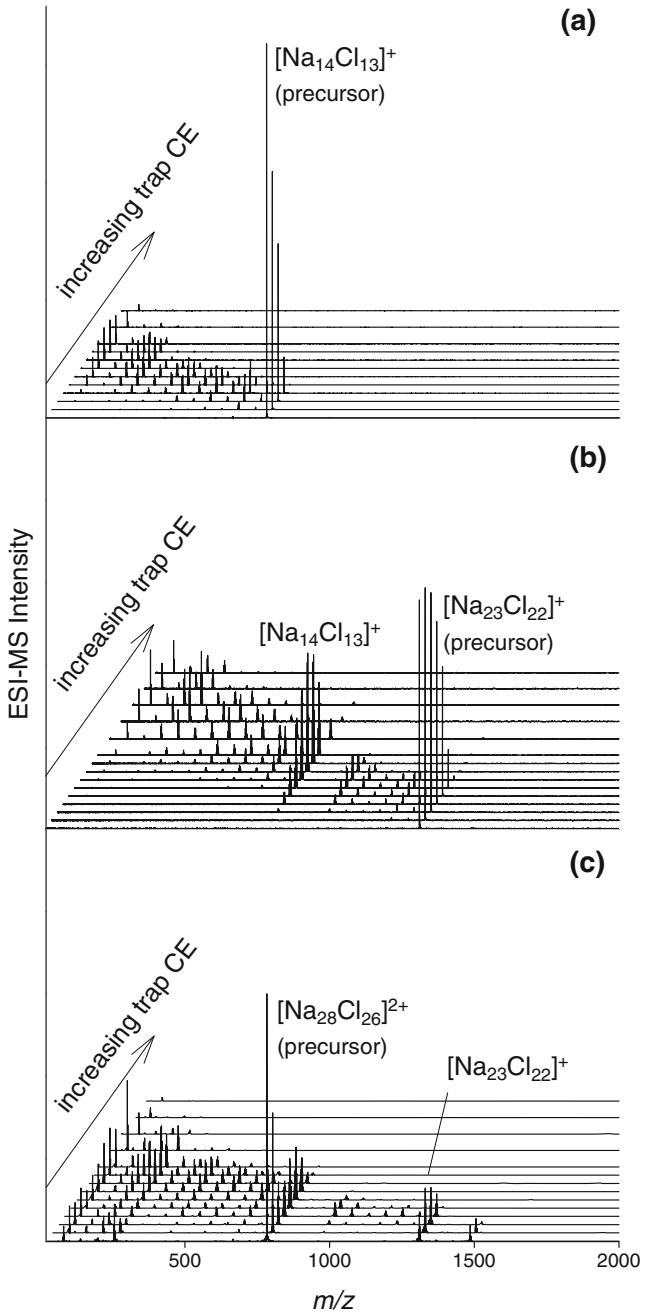

Figure 2. Tandem mass spectra of **(a)** $[Na_{14}Cl_{13}]^+$, **(b)** $[Na_{23}Cl_{22}]^+$, and **(c)** $[Na_{28}Cl_{26}]^{2+}$ acquired at different trap collision energies. In each panel, the spectrum with the lowest trap collision energy (4 V) is shown in the foreground. Trap collision energy values used: 4, 10, 15, 20, 25, 30, 35, 40, 45, 50, 60, 70, 80, 90, and 100 V

primarily via loss of small neutral $[NaCl]_i$ moieties. MD simulations qualitatively reproduce key features of the experimental CID behavior, offering insights into the temporal evolution of the collisionally excited clusters. Our data provide evidence of massive structural changes prior to fragmentation.

Experimental

Mass Spectrometry

ESI mass spectra were acquired on a Synapt G1 time-of-flight instrument (Waters, Milford, MA, USA). 10 mM NaCl in water was infused at 5 μL min^{-1} using a standard Z-spray source. The desolvation gas (N_2) temperature was set to 200 °C and the source block temperature was kept at 80 °C. In positive ion mode, the capillary voltage was set to 3 kV, and the extraction cone voltage was kept at 4 V. The sampling cone was set to 15 V for measurements on doubly charged clusters, and 75 V for singly charged species. The prevalence of singly charged clusters at elevated cone voltages has been noted previously [1]. In negative ion mode, the sampling and extraction cones were set to 30 and 5 V, respectively, whereas the capillary was operated at 2 kV. MS data represent the sum of 300 scans with an acquisition time of 1 s per spectrum.

MS/MS was conducted with quadrupole precursor ion selection, ensuring that only ions corresponding to a single isotope peak (the one with the highest signal intensity) were transmitted. These conditions ensured that doubly charged clusters could be interrogated without interferences from singly charged ions and vice versa. Fragmentation was induced by setting the trap collision energy to values between 4 and 100 V. CID was implemented with Ar as collision gas. MS/MS data for singly charged positive clusters were acquired with a scan time of 1 s for a total of 5 min. For fragmentation experiments on doubly charged clusters and for all negatively charged ions, the acquisition time was increased to 10 min per spectrum. Throughout this work we refer to positively charged clusters using the index n (such as $[Na_{(n+1)}Cl_n]^+$), whereas m is used to denote negative species ($[Na_mCl_{(m+1)}]^-$).

MD Simulations

Fragmentation trajectories were simulated using Gromacs 5.1 for leap frog integration of Newton's equations with a step size of Δt = 0.5 fs [60] and the Amber99sb-ILDN force field [61]. The choice of this force field is based on its successful use for earlier NaCl cluster ESI simulations [24]. Polarization effects are quite small for the types of ions considered here (particularly Na^+) [34, 57, 62, 63] thereby justifying the use of a nonpolarizable model. Simulations were performed in a vacuum environment without cut-offs for electrostatic or Lennard-Jones interactions [64]. As in previous CID simulations on other systems [54], the collision gas was not modeled explicitly because this would have caused a dramatic increase in the time required to complete the MD runs [48]. Instead, all simulations were conducted in constant temperature mode using the Nosé-Hoover thermostat [65]. This approach reflects the view that for many dissociation processes, the reaction outcome is not strongly dependent on the type of heating method employed (e.g., CID versus blackbody infrared dissociation [66]). Center of mass translation and rotation were eliminated throughout the simulations.

Positively charged $[Na_{(n+1)}Cl_n]^+$ clusters were generated using a previously generated $[Na_{14}Cl_{13}]^+$ (3 × 3 × 3) cubic structure as point of origin [24]. For producing $[Na_{23}Cl_{22}]^+$ and

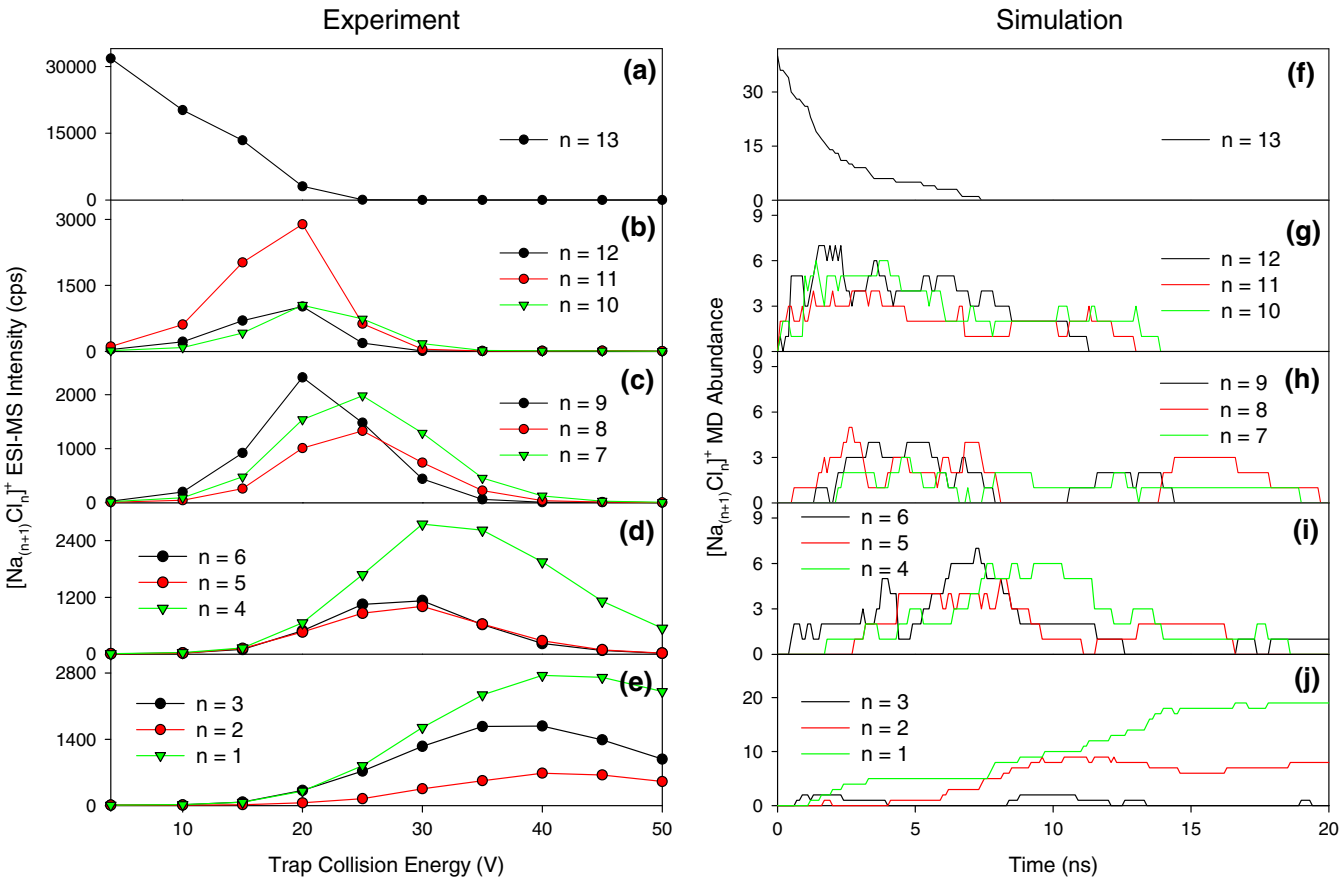

Figure 3. **(a)–(e)** Experimental intensities of $[Na_{(n+1)}Cl_n]^+$ product ions observed after fragmentation of $[Na_{14}Cl_{13}]^+$ at various trap collision energies. **(f)–(j)** MD simulation data displaying the abundance of various $[Na_{(n+1)}Cl_n]^+$ species during fragmentation cascades starting with $[Na_{14}Cl_{13}]^+$. The profiles were compiled from 40 independent runs

$[Na_{28}Cl_{26}]^{2+}$, the corresponding number of Na^+ and Cl^- ions were added in random positions less than 1 nm from this $[Na_{14}Cl_{13}]^+$ core. These structures were then annealed by consecutive 10 ps runs at 500, 400, 200, 100, 50, 1 K. This was followed by another 10 ns equilibration period at 300 K. Negative clusters were obtained by inversion of cation and anion positions, followed by steepest descent energy minimization.

Extensive test runs were conducted for identifying a suitable simulation temperature. Temperatures around 1200 K and below were found to cause some structural dynamics but virtually no dissociation over many nanoseconds. All data shown below were thus generated at 1400 K, which produced readily observable CID events on a ns time scale. For reference, it is noted that these simulation conditions lie between the melting temperature (1038 K) and the boiling temperature (1738 K) of bulk NaCl [67]. Production runs were broken down into segments. The length of each segment was governed by the time required for the charged precursor cluster to undergo dissociation. After removal of the neutral dissociation product, the run was restarted using the residual charged fragment as new starting structure. The maximum run time for each segment was 20 ns. Simulated product ion distributions represent the average of forty independent runs for each cluster type, each generated with different initial velocities that were sampled at random from a Maxwell-Boltzmann distribution. Graphics were rendered using Pymol. Ions are represented with their van der Waals radii (i.e., 1.02 Å for Na^+ and 1.81 Å for Cl^-) [67].

Results and Discussion

MS of Aqueous NaCl Solutions

In agreement with previous reports [1, 3, 8, 34, 43], we found that ESI of aqueous NaCl solution in positive ion mode produces a range of $[Na_{(n+1)}Cl_n]^+$ clusters, with elevated abundance for the $n = 4$, 13, and 22 magic number species (Figure 1). Low intensity doubly charged clusters became observable upon lowering the cone voltage from 75 to 15 V [1] (Figure 1, insert). Also shown in Figure 1 are ground state ($T = 1$ K) structures of magic number clusters predicted by MD simulations. The cuboid shapes of the $n = 4$, 13, and 22 singly charged species are consistent with the results of previous experimental and theoretical investigations [1, 22, 37, 38]. For the doubly charged cluster $[Na_{28}Cl_{26}]^{2+}$, our MD simulations predict a rhomboid ground state structure (Figure 1) that is in agreement with the results of ab initio calculations [39]. These data do not support the proposal [34] that $[Na_{28}Cl_{26}]^{2+}$ is a composite of

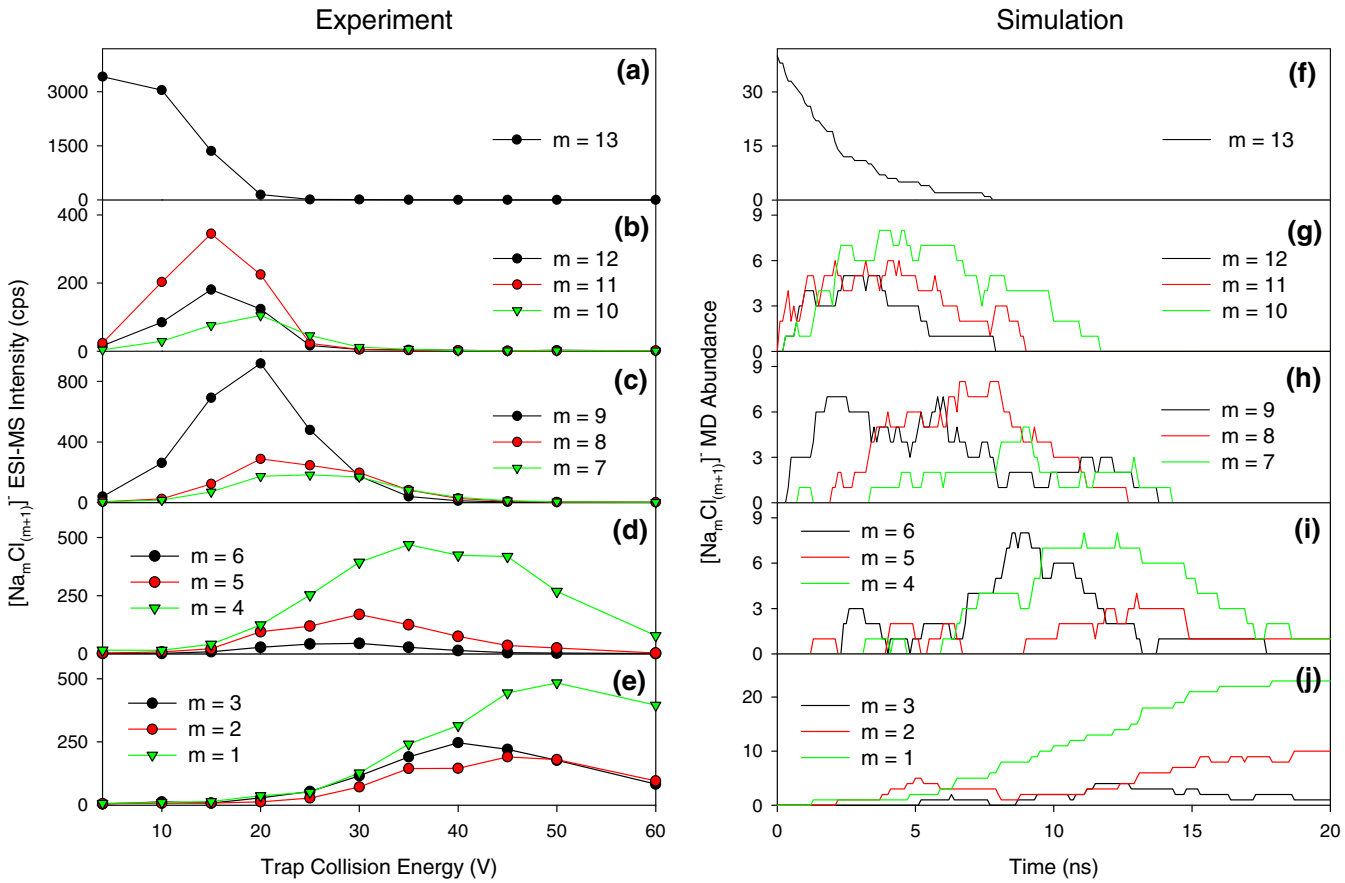

Figure 4. **(a)–(e)** Experimental intensities of $[Na_mCl_{(m+1)}]^-$ product ions observed after fragmentation of $[Na_{13}Cl_{14}]^-$, analogous to Figure 3. The corresponding MD simulation data are shown in **(f)–(j)**

two cuboid units. Switching to negative ESI resulted in a progression of singly charged $[Na_mCl_{(m+1)}]^-$ clusters similar to that of Figure 1, although with a somewhat different intensity pattern (Supporting Information Figure S1).

MS/MS of Singly Charged Clusters

CID of $[Na_{14}Cl_{13}]^+$ generates a ladder of $[Na_{(n+1)}Cl_n]^+$ product ions with $n = 12$, 11, 10, … (Figure 2a). With increasing collision energy, the size distribution gradually shifts to smaller species, all the way to $[Na_2Cl]^+$ ($n = 1$) as the dominant product ion under the harshest conditions used (Figure 3a–e). Clearly, the entire fragmentation cascade is dominated by the loss of small neutrals. The simplest interpretation of these MS/MS data is a sequential progression with [NaCl] loss in each step (i.e., $[Na_{14}Cl_{13}]^+ \rightarrow [Na_{13}Cl_{12}]^+ \rightarrow [Na_{12}Cl_{11}]^+ \rightarrow \ldots \rightarrow [Na_2Cl]^+$). The actual situation is likely more complex because the ejection of other small neutrals such as $[NaCl]_2$ and $[NaCl]_3$ cannot be ruled out [43]. Qualitatively similar behavior was seen in negative ESI experiments on $[Na_{13}Cl_{14}]^-$ (Figure 4a–e, Supporting Information Figure S2a).

MS/MS was also conducted on the $n = 22$ singly charged cluster $[Na_{23}Cl_{22}]^+$ (Figure 2b, Supporting Information Figure S3a-e). As in the cases above, increasing collision energies induced gradual shifts in the product ion distribution towards smaller n. Interestingly, the $n = 13$ magic number cluster $[Na_{14}Cl_{13}]^+$ has an unusually high abundance. The prevalence of this CID intermediate indicates that clusters slightly larger than this magic number species exhibit reduced kinetic stability. Indeed, $[Na_{15}Cl_{14}]^+$ and $[Na_{16}Cl_{15}]^+$ are virtually undetectable in Figure 2b, suggesting that they rapidly convert to the $n = 13$ magic number cluster via [NaCl] ejection, thereby boosting the $[Na_{14}Cl_{13}]^+$ abundance. Despite these nuances, the general picture emerging from the MS/MS data in Figure 2 is that collisional excitation causes the sequential loss of [NaCl], and likely also $[NaCl]_2$ and $[NaCl]_3$. The negative $[Na_{22}Cl_{23}]^-$ cluster shows the same general CID trends (Supporting Information Figures S2b, S4).

All of the singly charged cluster ions examined here break down via a sequential progression of small neutral losses upon collisional activation [43]. This is not a trivial observation because other types of CID processes could be envisioned as well. Examples of hypothetical alternative scenarios include Na^+ ejection to produce large neutral species, or cluster splitting into charged/neutral product pairs of comparable size. The fragmentation behavior observed here for NaCl cluster ions is similar to that of other salt clusters [7, 44].

MD Simulations of Singly Charged Clusters

Different $[Na_{(n+1)}Cl_n]^+$ and $[Na_mCl_{(m+1)}]^-$ species were simulated in a vacuum environment to gain insights into the

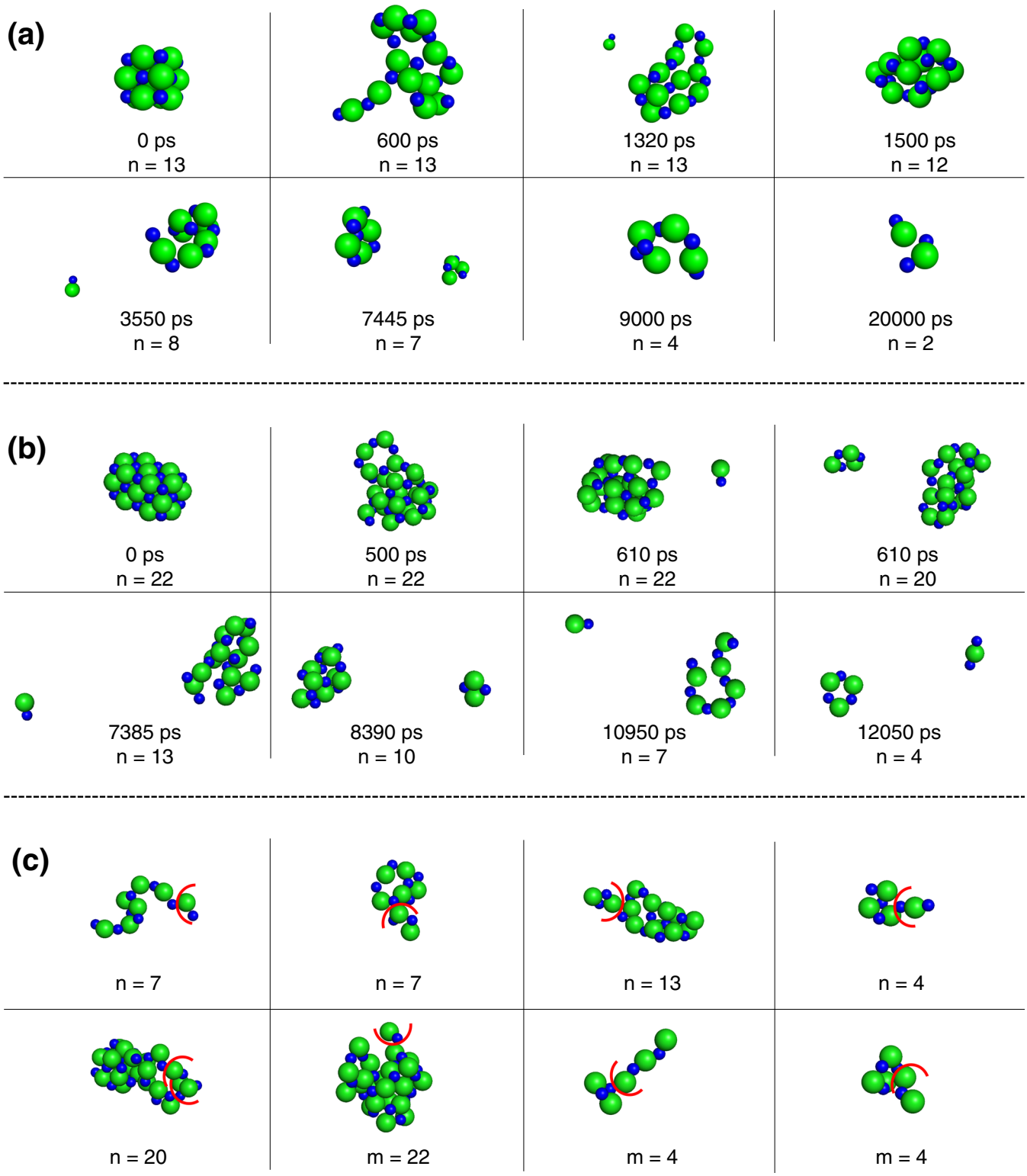

Figure 5. **(a)** Structural snapshots taken from an MD trajectory of the stepwise fragmentation of a $[Na_{14}Cl_{13}]^+$ cluster. The initial ground state is shown in the top left corner. Values of n in each panel refer to the total number of ions, regardless of whether the $[Na_{(n+1)}Cl_n]^+$ clusters are intact or have undergone dissociation. **(b)** Same as in panel A, but for fragmentation of $[Na_{23}Cl_{22}]^+$. **(c)** MD transition state structures just prior to ejection of $(NaCl)_i$ ($i = 1, 2, 3$) from various clusters. The data represent time points taken from different trajectories. Red lines indicate where dissociation is about to take place. The total cluster size is indicated in each panel; n refers to $[Na_{(n+1)}Cl_n]^+$, m refers to $[Na_mCl_{(m+1)}]^-$

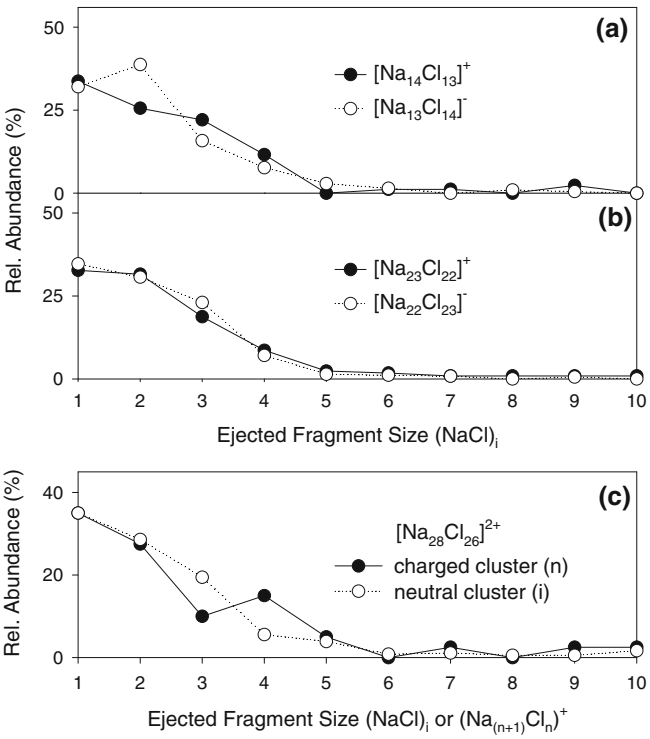

Figure 6. Size distributions of ejected fragments observed in MD runs starting with different magic number clusters. The data refer to products generated during the entire fragmentation cascade (i.e., not just during decomposition of the original precursor ion). **(a)**, **(b)**: runs starting with singly charged positive and negative magic number clusters, as indicated in each panel. **(c)** Fragmentation runs starting with $[Na_{28}Cl_{26}]^{2+}$

dynamics of these clusters under CID conditions. As an example, MD snapshots taken at selected time points during a run starting with $[Na_{14}Cl_{13}]^+$ are depicted in Figure 5a. Thermal excitation transforms the cuboid ground state into a highly dynamic system that fluctuates between various compact and more extended structures. The cluster gradually shrinks by ejection of neutral moieties, mostly [NaCl], $[NaCl]_2$, and $[NaCl]_3$. Very similar events are seen during simulation runs starting with the larger cluster $[Na_{23}Cl_{22}]^+$ (Figure 5b). Analysis of the simulated CID cascades reveals sequential shifts in $[Na_{(n+1)}Cl_n]^+$ fragment ion populations towards lower values of n (Figure 3f–j). Analogous behavior was observed in MD simulations conducted on $[Na_{22}Cl_{23}]^-$ (Figure 4f–j) and for larger clusters both in positive and in negative ion mode (Supporting Information Figures S3, S4).

Although the simulated fragment ion populations in Figures 3 and 4, and Supporting Information Figures S3, S4 do not exactly match the experimental data, several general trends are well reproduced: (1) The simulated trajectories show a charged parent cluster that gradually shrinks. (2) Excess charge is retained on the larger dissociation product for almost all of the fission events. (3 Ejection of small $[NaCl]_i$ neutrals is the dominant dissociation pathway. This last point is emphasized in Figure 6a and b, where data were compiled for a total of 160 MD runs on $[Na_{14}Cl_{13}]^+$, $[Na_{23}Cl_{22}]^+$, $[Na_{13}Cl_{14}]^-$, and $[Na_{22}Cl_{23}]^-$. These data reveal that ~80% of all simulated dissociation events correspond to loss of $[NaCl]_i$, with $i = 1, 2, 3$. The fact that these key features of the simulations are consistent with the experimental behavior implies that our MD data provide a reasonable overall description of the $[Na_{(n+1)}Cl_n]^+$ and $[Na_mCl_{(m+1)}]^-$ dynamics under CID conditions.

An important question is *why* loss of small neutrals is the dominant CID pathway for singly charged parent clusters. This aspect can be answered by looking at the MD transition state structures exemplified in Figure 5c, which represent clusters that are just about to release a small $[NaCl]_i$ moiety. Most dissociation events take place during brief instances where the clusters adopt a relatively compact core structure with a short protruding $[NaCl]_i$ appendix. These deformed structures are primed for dissociation because the small $[NaCl]_i$ moieties can separate from the complex via thermally activated rupture of a *single* Na-Cl contact (indicated by the red lines in Figure 5c). Only on rare occasions did we observe product release after rupture of two such contacts (exemplified by the $n = 20$ structure in Figure 5c). Single bond cleavage events are kinetically preferred over processes that involve the quasi-simultaneous rupture of multiple electrostatic contacts. The latter scenario could potentially produce larger fragments, but such reaction pathways are disfavored because of their higher activation barriers [68].

CID of $[Na_{28}Cl_{26}]^{2+}$

$[Na_{28}Cl_{26}]^{2+}$ was the only doubly charged species that could be studied with satisfactory S/N ratio in our experiments. When applying low collision energies the symmetrical dissociation into equal singly charged magic number fragments, $[Na_{14}Cl_{13}]^+$ was found to be the dominant reaction pathway. Asymmetric cleavage into the magic number species $[Na_{23}Cl_{22}]^+$ and $[Na_5Cl_4]^+$ occurred to a lesser extent. Sequential small neutral losses at elevated collision energies likely reflect secondary dissociation of primary fragment ions, rather than decomposition of the doubly charged precursor (Figure 2c and Supporting Information Figure S5).

The agreement between these experimental data for $[Na_{28}Cl_{26}]^{2+}$ and the corresponding MD simulations is not as good as for the singly charged clusters discussed earlier. Simulations of $[Na_{28}Cl_{26}]^{2+}$ predict the ejection of small $[NaCl]_i$ neutrals and small singly charged $[Na_{(n+1)}Cl_n]^+$ clusters as the dominant fragmentation pathways (Figure 6c and Supporting Information Figure S5). Encouragingly, the elevated abundance of the $n = 4$ fragmentation channel in the MD data (Figure 6c) corresponds to the experimentally observed $[Na_{28}Cl_{26}]^{2+}$ decomposition into $[Na_{23}Cl_{22}]^+$ and $[Na_5Cl_4]^+$. Also, we note that the ejection of small singly charged fragments (as predicted in Figure 6c) does indeed take place for the $z = 2$ clusters of some other salts [69].

Despite the limited ability of MD simulations to capture the experimentally observed behavior of $[Na_{28}Cl_{26}]^{2+}$, our data nonetheless allow some basic conclusions to be drawn regarding the CID mechanism of this species. Previous work implied that fragmentation of doubly charged clusters can be interpreted as shattering into preformed singly charged magic number blocks

[34]. The experimentally observed dominant CID pathway $[Na_{28}Cl_{26}]^{2+} \rightarrow 2\ [Na_{14}Cl_{13}]^{+}$ cannot be explained by such a model because it is geometrically impossible to assemble two $[Na_{14}Cl_{13}]^{+}$ $(3 \times 3 \times 3)$ cubes into a $(3 \times 3 \times 3)_2$ parent structure without creating unfavorable Na^{+}/Na^{+} and Cl^{-}/Cl^{-} nearest neighbor contacts. The actual $[Na_{28}Cl_{26}]^{2+}$ ground state has a rhomboid structure [39] (Figure 1) that does not lend itself to simple cleavage into cuboid building blocks. In addition, the occurrence of major structural changes prior to dissociation [45] makes it unlikely that product ions can retain structural features that originate directly from the precursor ground state. The mechanism whereby collisional excitation of $[Na_{28}Cl_{26}]^{2+}$ generates singly charged fragments with magic number compositions thus remains unresolved.

Conclusions

Despite their simple chemical nature, ESI-generated $[Na_xCl_y]^{(x-y)+}$ clusters exhibit a rich fragmentation behavior. These clusters provide an excellent testbed for evaluating the suitability of computational methods for elucidating fundamental aspects of CID processes. To the best of our knowledge, the current work marks the first time that MD methods were applied to examine the mechanistic pathways whereby collisionally heated salt clusters undergo dissociation.

Consistent with the results of IMS investigations [45], our data reveal the occurrence of major structural fluctuations before decomposition events take place. This finding implies that none of the dissociation products can retain direct memory of the ground state precursor structures. The observed behavior bears interesting parallels to CID processes of multi-protein complexes, where extensive unfolding ("melting") of the native structure takes place prior to disintegration [30, 54, 70].

It is gratifying that our MD simulations successfully capture key features of the experimentally observed CID behavior for singly charged $[Na_xCl_y]^{(x-y)+}$ clusters. In particular, the simulations explain why the loss of small neutral $[NaCl]_i$ moieties represents the dominant fragmentation channel. The MD trajectories reveal that these neutral products are formed from transiently populated cluster structures that bear a small $[NaCl]_i$ protrusion. The latter can then separate from the cluster via rupture of a single Na-Cl contact. Fragmentation events of this type are kinetically favored over other pathways that would require the quasi-simultaneous rupture of multiple electrostatic contacts, corresponding to larger activation barriers.

In the case of the doubly charged species $[Na_{28}Cl_{26}]^{2+}$, the agreement between experiments and MD simulations was not as good. It seems possible that a realistic description of multiply charged clusters requires more elaborate MD strategies, with inclusion of polarizability effects and the presence of an explicit collision gas [48]. Work in this direction is currently ongoing in our laboratory, as well as experimental studies and simulations on cluster ions consisting of salts other than NaCl. The results of these efforts will be reported elsewhere.

Acknowledgments

Funding for this work was provided by the Natural Sciences and Engineering Research Council of Canada (Discovery Grant 217080–2013).

References

1. Hao, C.Y., March, R.E., Croley, T.R., Smith, J.C., Rafferty, S.P.: Electrospray ionization tandem mass spectrometric study of salt cluster ions. Part 1 – Investigations of alkali metal chloride and sodium salt cluster ions. J. Mass Spectrom. **36**, 79–96 (2001)
2. Hao, C.Y., March, R.E.: Electrospray ionization tandem mass spectrometric study of salt cluster ions: Part 2 – Salts of polyatomic acid groups and of multivalent metals. J. Mass Spectrom. **36**, 509–521 (2001)
3. Wakisaka, A.: Nucleation in alkali metal chloride solution observed at the cluster level. Faraday Discuss. **136**, 299–308 (2007)
4. Wang, G.D., Cole, R.B.: Solvation energy and gas-phase stability influences on alkali metal cluster ion formation in electrospray ionization mass spectrometry. Anal. Chem. **70**, 873–881 (1998)
5. Gamero-Castano, M., de la Mora, J.F.: Modulations in the abundance of salt clusters in electrosprays. Anal. Chem. **72**, 1426–1429 (2000)
6. Zook, D.R., Bruins, A.P.: On cluster ions, ion transmission, and linear dynamic range limitations in electrospray (ionspray) mass spectrometry. Int. J. Mass Spectrom. Ion Processes **162**, 129–147 (1997)
7. Ouyang, H., Larriba-Andaluz, C., Oberreit, D.R., Hogan, C.J.: The collision cross sections of iodide salt cluster ions in air via differential mobility analysis-mass spectrometry. J. Am. Soc. Mass Spectrom. **24**, 1833–1847 (2013)
8. Hop, C.E.C.A.: Generation of high molecular weight cluster ions by electrospray ionization; implications for mass calibration. J. Mass Spectrom. **31**, 1314–1316 (1996)
9. Mahler, J., Persson, I.: A study of the hydration of the alkali metal ions in aqueous solution. Inorg. Chem. **51**, 425–438 (2012)
10. Meng, C.K., Fenn, J.B.: Formation of charged clusters during electrospray ionization of organic solute species. Org. Mass Spectrom. **26**, 542–549 (1991)
11. Nanita, S.C., Cooks, R.G.: Serine octamers: cluster formation, reactions, and implications for biomolecule homochirality. Angew. Chem. Int. Ed. **45**, 554–569 (2006)
12. Julian, R.R., Hodyss, R., Kinnear, B., Jarrold, M.F., Beauchamp, J.L.: Nanocrystalline aggregation of serine detected by electrospray ionization mass spectrometry: origin of the stable homochiral gas-phase serine octamer. J. Phys. Chem. B **106**, 1219–1228 (2002)
13. Do, T.D., de Almeida, N.E.C., LaPointe, N.E., Chamas, A., Feinstein, S.C., Bowers, M.T.: Amino acid metaclusters: implications of growth trends on peptide self-assembly and structure. Anal. Chem. **88**, 868–876 (2016)
14. Kebarle, P., Peschke, M.: On the mechanisms by which the charged droplets produced by electrospray lead to gas phase ions. Anal. Chim. Acta **406**, 11–35 (2000)
15. Wang, G., Cole, R.B.: Charged residue versus ion evaporation for formation of alkali metal halide clusters ions in ESI. Anal. Chim. Acta **406**, 53–65 (2000)
16. Blades, A.T., Peschke, M., Verkerk, U.H., Kebarle, P.: Hydration energies in the gas phase of select (MX)(m)M+ ions, where M+=Na+, K+, Rb+, Cs+, NH4(+), and X-=F-, Cl, Br-, I-, NO2-, NO3-.Observed magic numbers of (MX)(m)M+ ions and their possible significance. J. Am. Chem. Soc. **126**, 11995–12003 (2004)
17. Spencer, E.A.C., Ly, T., Julian, R.K.: Formation of the serine octamer: Ion evaporation or charge residue? Int. J. Mass Spectrom. **270**, 166–172 (2008)
18. Iribarne, J.V., Thomson, B.A.: On the evaporation of small ions from charged droplets. J. Chem. Phys. **64**, 2287–2294 (1976)
19. Znamenskiy, V., Marginean, I., Vertes, A.: Solvated ion evaporation from charged water droplets. J. Phys. Chem. A **107**, 7406–7412 (2003)
20. Konermann, L., Ahadi, E., Rodriguez, A.D., Vahidi, S.: Unraveling the mechanism of electrospray ionization. Anal. Chem. **85**, 2–9 (2013)
21. Consta, S., Mainer, K.R., Novak, W.: Fragmentation mechanisms of aqueous clusters charged with ions. J. Chem. Phys. **119**, 10125–10132 (2003)

22. Juraschek, R., Dulcks, T., Karas, M.: Nanoelectrospray – more than just a minimized-flow electrospray ionization source. J. Am. Soc. Mass Spectrom. **10**, 300–308 (1999)
23. Zhou, S., Hamburger, M.: Formation of sodium cluster ions in electrospray mass spectrometry. Rapid Commun. Mass Spectrom. **10**, 797–800 (1996)
24. Konermann, L., McAllister, R.G., Metwally, H.: Molecular dynamics simulations of the electrospray process: formation of NaCl clusters via the charged residue mechanism. J. Phys. Chem. B **118**, 12025–12033 (2014)
25. Dole, M., Mack, L.L., Hines, R.L., Mobley, R.C., Ferguson, L.D., Alice, M.B.: Molecular beams of macroions. J. Chem. Phys. **49**, 2240–2249 (1968)
26. Kebarle, P., Verkerk, U.H.: Electrospray: from ions in solutions to ions in the gas phase, what we know now. Mass Spectrom. Rev. **28**, 898–917 (2009)
27. Verkerk, U.H., Kebarle, P.: Ion–ion and ion–molecule reactions at the surface of proteins produced by nanospray. information on the number of acidic residues and control of the number of ionized acidic and basic residues. J. Am. Soc. Mass Spectrom. **16**, 1325–1341 (2005)
28. Grewal, R.N., El Aribi, H., Smith, J.C., Rodriquez, C.F., Hopkinson, A.C., Siu, K.W.M.: Multiple substitution of protons by sodium ions in sodiated oligoglycines. Int. J. Mass Spectrom. **219**, 89–99 (2002)
29. Hu, P., Ye, Q.-Z., Loo, J.A.: Calcium stoichiometry determination for calcium binding proteins by electrospray ionization mass spectrometry. Anal. Chem. **66**, 4190–4194 (1994)
30. Han, L., Hyung, S.-J., Ruotolo, B.T.: Bound cations significantly stabilize the structure of multiprotein complexes in the gas phase. Angew. Chem. Int. Ed. **51**, 5692–5695 (2012)
31. Wagner, N.D., Kim, D., Russell, D.H.: Increasing ubiquitin ion resistance to unfolding in the gas phase using chloride adduction: preserving more "native-like" conformations despite collisional activation. Anal. Chem. **in press**, DOI: 10.1021/acs.analchem.6b00871 (2016)
32. McAllister, R.G., Metwally, H., Sun, Y., Konermann, L.: Release of native-like gaseous proteins from electrospray droplets via the charged residue mechanism: insights from molecular dynamics simulations. J. Am. Chem. Soc. **137**, 12667–12676 (2015)
33. Liu, X., Cole, R.B.: "Best Match" model and effect of na+/h + exchange on anion attachment to peptides and stability of formed adducts in negative ion electrospray mass spectrometry. J. Am. Soc. Mass Spectrom. **25**, 204–213 (2014)
34. Zhang, D.X., Cooks, R.G.: Doubly charged cluster ions (NaCl)(m)(Na)(2) (2+): magic numbers, dissociation, and structure. Int. J. Mass Spectrom. **195**, 667–684 (2000)
35. Lee, S.W., Freivogel, P., Schindler, T., Beauchamp, J.L.: Freeze-dried biomolecules: FT-ICR studies of the specific solvation of functional groups and clathrate formation observed by the slow evaporation of water from hydrated peptides and model compounds in the gas phase. J. Am. Chem. Soc. **120**, 11758–11765 (1998)
36. Rodriguez-Cruz, S.E., Klassen, J.S., Williams, E.R.: Hydration of gas-phase gramicidin S (M + 2H)(2+) ions formed by electrospray: the transition from solution to gas-phase structure. J. Am. Soc. Mass Spectrom. **8**, 565–568 (1997)
37. Doye, J.P.K., Wales, D.E.: Structural transitions and global minima of sodium chloride clusters. Phys. Rev. B 2292–2300 (1999)
38. Phillips, N.G., Conover, C.W.S., Bloomfield, L.A.: Calculations of the binding energies and structures of sodium chloride clusters and cluster ions. J. Chem. Phys. **94**, 4980–4987 (1991)
39. Aguado, A.: An ab initio study of the structures and relative stabilities of doubly charged (NaCl)(m)(Na)(2) (2+) cluster ions. J. Phys. Chem. B **105**, 2761–2765 (2001)
40. Brodbelt, J.S.: Ion activation methods for peptides and proteins. Anal. Chem. **88**, 30–51 (2016)
41. Mayer, P.M., Poon, C.: The mechanism of collisional activation of ions in mass spectrometry. Mass Spectrom. Rev. **28**, 608–639 (2009)
42. Sleno, L., Volmer, D.A.: Ion activation methods for tandem mass spectrometry. J. Mass Spectrom. **39**, 1091–1112 (2004)
43. Feketeova, L., O'Hair, R.A.J.: Comparison of collision- versus electron-induced dissociation of sodium chloride cluster cations. Rapid Commun. Mass Spectrom. **23**, 60–64 (2009)
44. Hogan, C.J., de la Mora, J.F.: Ion-pair evaporation from ionic liquid clusters. J. Am. Soc. Mass Spectrom. **21**, 1382–1386 (2010)
45. Hudgins, R.R., Dugourd, P., Tenenbaum, J.M., Jarrold, M.F.: Structural transitions in sodium chloride nanocrystals. Phys. Rev. Lett. **78**, 4213–4216 (1997)
46. Higashi, H., Tokumi, T., Hogan, C.J., Suda, H., Seto, T., Otani, Y.: Simultaneous ion and neutral evaporation in aqueous nanodrops: experiment, theory, and molecular dynamics simulations. Phys. Chem. Chem. Phys. **17**, 15746–15755 (2015)
47. Consta, S., Oh, M.I., Soltani, S.: Advances in the theoretical and molecular simulation studies of the ion chemistry in droplets. Int. J. Mass Spectrom. **377**, 557–567 (2015)
48. Daub, C.D., Cann, N.M.: How are completely desolvated ions produced in electrospray ionization: insights from molecular dynamics simulations. Anal. Chem. **83**, 8372–8376 (2011)
49. Mao, Y., Woenckhaus, J., Kolafa, J., Ratner, M.A., Jarrold, M.F.: Thermal unfolding of unsolvated cytochrome *c*: experiment and molecular dynamics simulations. J. Am. Chem. Soc. **121**, 2712–2721 (1999)
50. Khakinejad, M., Kondalaji, S.G., Maleki, H., Arndt, J.R., Donohoe, G.C., Valentine, S.J.: Combining ion mobility spectrometry with hydrogen-deuterium exchange and top-down MS for peptide ion structure analysis. J. Am. Soc. Mass Spectrom. **25**, 2103–2115 (2014)
51. Hall, Z., Politis, A., Bush, M.F., Smith, L.J., Robinson, C.V.: Charge-state dependent compaction and dissociation of protein complexes: insights from ion mobility and molecular dynamics. J. Am. Chem. Soc. **134**, 3429–3438 (2012)
52. Patriksson, A., Adams, C.M., Kjeldsen, F., Zubarev, R.A., van der Spoel, D.: A direct comparison of protein structure in the gas and solution phase: the TRP-cage. J. Phys. Chem. B **111**, 13147–13150 (2007)
53. Steinberg, M.Z., Elber, R., McLafferty, F.W., Gerber, R.B., Breuker, K.: Early structural evolution of native cytochrome *c* after solvent removal. Chem. BioChem. **9**, 2417–2423 (2008)
54. Fegan, S.K., Thachuk, M.: A charge moving algorithm for molecular dynamics simulations of gas-phase proteins. J. Chem. Theory Comput. **9**, 2531–2539 (2013)
55. Chen, S.-H., Russell, D.H.: How closely related are conformations of protein ions sampled by IM-MS to native solution structures? J. Am. Soc. Mass Spectrom. **26**, 1433–1443 (2015)
56. Larriba, C., de la Mora, J.F.: The gas phase structure of coulombically stretched polyethylene glycol ions. J. Phys. Chem. B **116**, 593–598 (2011)
57. Kohagen, M., Mason, P.E., Jungwirth, P.: Accounting for electronic polarization effects in aqueous sodium chloride via molecular dynamics aided by neutron scattering. J. Phys. Chem. B **120**, 1454–1460 (2016)
58. Fuentes-Azcatl, R., C., B.M.: Sodium chloride, NaCl/ϵ: new force field. J. Phys. Chem. B **in press** (2016)
59. Moucka, F., Nezbeda, I., Smith, W.R.: Molecular force fields for aqueous electrolytes: SPC/E-compatible charged LJ sphere models and their limitations. J. Chem. Phys. **138** (2013)
60. Hess, B., Kutzner, C., van der Spoel, D., Lindahl, E.: GROMACS 4: Algorithms for highly efficient, load-balanced, and scalable molecular simulation. J. Chem. Theory Comput. **4**, 435–447 (2008)
61. Lindorff-Larsen, K., Piana, S., Palmo, K., Maragakis, P., Klepeis, J.L., Dror, R.O., Shaw, D.E.: Improved side-chain torsion potentials for the Amber ff99SB protein force field. Proteins **78**, 1950–1958 (2010)
62. Sternheimer, R.M.: Electronic polarizabilities of ions. Phys. Rev. **107**, 1565–1569 (1957)
63. Pyper, N.C., Popelier, P.: The polarizabilities of halide ions in crystals. J. Phys.-Cond. Matt. **9**, 471–488 (1997)
64. Caleman, C., van der Spoel, D.: Temperature and structural changes of water clusters in vacuum due to evaporation. J. Chem. Phys. **125**, 1545081–1545089 (2006)
65. Hoover, W.G.: Canonical dynamics: equilibrium phase-space distributions. Phys. Rev. A **31**, 1695–1697 (1985)
66. Felitsyn, N., Kitova, E.N., Klassen, J.S.: Thermal decomposition of a gaseous multiprotein complex studied by Blackbody infrared radiative dissociation Investigating the origin of the asymmetric dissociation behavior. Anal. Chem. **73**, 4647–4661 (2001)
67. Lide, D.R.: CRC Handbook of Chemistry and Physics, 82nd edn. CRC Press, Boca Raton, London, New York, Washington (2001)
68. Hanggi, P., Talkner, P., Borkovec, M.: Reaction-rate theory: fifty years after Kramers. Rev. Mod. Pys. **62**, 251–342 (1990)
69. Hogan, C.J., de la Mora, J.F.: Tandem ion mobility-mass spectrometry (IMS-MS) study of ion evaporation from ionic liquid-acetonitrile nanodrops. Phys. Chem. Chem. Phys. **11**, 8079–8090 (2009)
70. Quintyn, R.S., Zhou, M., Yan, J., Wysocki, V.H.: Surface-induced dissociation mass spectra as a tool for distinguishing different structural forms of gas-phase multimeric protein complexes. Anal. Chem. **87**, 11879–11886 (2015)